

Algebraic Weighting Factor Selection for Predictive Torque and Flux Control

Tobias Geyer, *Senior Member, IEEE*

Abstract—The cost function of finite control set model predictive torque and flux control uses a weighting factor to determine the trade-off between the torque and flux magnitude tracking errors. The choice of this weighting factor strongly influences the current distortions. It will be shown that the optimal weight, which minimizes the current distortions, can be computed algebraically. Furthermore, using this weighting factor, the predictive torque and flux controller achieves a current distortion per switching frequency that is very similar to that of predictive current control. To achieve this similar performance, the corresponding weighting factors on the switching effort need to be selected appropriately. To this end, a second analytical expression will be derived.

I. INTRODUCTION

Finite control set model predictive control (FCS-MPC) has become popular thanks to its versatility, and its algorithmic and computational simplicity [1]. In order to achieve the desired closed-loop performance characteristic, however, the weighting factors in the cost function need to be selected carefully. This tuning process is usually performed on a trial-and-error basis [2] and is thus considered an unresolved issue [3].

An important member of the FCS-MPC family is predictive torque and flux control [4] for variable speed drives. By *directly* controlling the electromagnetic torque and the machine magnetization, a high degree of robustness can be achieved [5]. The predicted torque and stator flux magnitude errors are penalized in the cost function. To determine the relative importance of these two terms, a weighting factor is introduced. The latter has a significant impact on the control performance, particularly on the harmonic current distortions.

To select the weighting factors in FCS-MPC, the predominantly used approach is to run multiple closed-loop simulations for a range of weights and to then choose the combination of weights that minimizes a given performance criterium [6]–[9]. To simplify this process, it is advisable to normalize the controlled quantities [6], for example by adopting a per unit system. To speed up the selection process, optimization methods can be used to derive Pareto fronts, see [10].

On the other hand, an algebraic method was proposed in [11] for predictive torque and flux control when applied to two-level inverters; when alternating between active and zero vectors, analytical expressions for the weighting factors can be derived that minimize the torque ripple. By ranking the magnitude of each cost function term and then taking the minimum of their average value, the weighting factors can be

avoided altogether [12]. In effect, this leads to a discrete cost function, but nevertheless requires the tuning of the relative importance of the flux with respect to the torque.

Alternatively, by adopting the notion of field orientation [13], the torque and machine magnetization can be controlled *indirectly* through orthogonal stator current components using the notion of predictive current control. This concept was introduced in [14] and later refined in [15]–[17]. It is generally accepted that the two orthogonal current components should be equally penalized to minimize the current distortions, see also [18] and [19]. To reduce the switching frequency, the predicted number of commutations should also be penalized in the cost function. The associated trade-off between current tracking and switching frequency is fundamental to power electronics and well understood, see for example [20].

This paper aims to further the understanding of the weighting factor selection process in predictive torque and flux control by answering two questions: First, what are the optimal weighting factors on the torque and flux error terms that achieve minimal current distortions for a given switching frequency? It turns out that a simple analytical expression can be derived.

Second, is it possible to tune the predictive torque controller such that it becomes equivalent to the predictive current controller in terms of the current distortions per switching frequency? An analysis of the cost function level sets shows that this is in general impossible, but an analytical expression for the weighting factors can nevertheless be derived that makes both controllers perform in as similar a manner as possible.

For illustrative purposes, a medium-voltage (MV) drive system with a three-level neutral point clamped (NPC) inverter and an induction machine will be considered. To simplify the exposition, the neutral point potential will be assumed to be zero, and a per unit system will be adopted to normalize all quantities. We will restrict the prediction horizon to one step, as this variant of FCS-MPC is the most widely used one.

II. DRIVE SYSTEM CASE STUDY

Consider an NPC voltage source inverter connected to an MV induction machine, as shown in Fig. 1. A 3.3 kV and 50 Hz squirrel-cage induction machine rated at 2 MVA is used. The dc-link voltage is $V_{dc} = 5.2$ kV and assumed to be constant. The potential of the neutral point N is fixed to zero. The detailed parameters of the machine and inverter are summarized in Table I.

The author is with ABB Corporate Research, Baden-Dättwil, Switzerland; e-mail: t.geyer@ieee.org

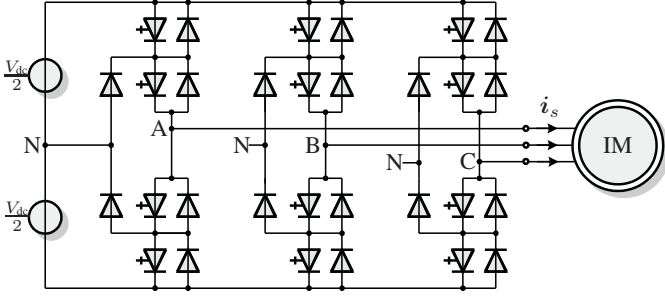


Fig. 1: NPC inverter with an induction motor and a fixed neutral point potential

Throughout the paper, we will use normalized quantities. The per unit (pu) system is established using the base quantities $V_B = \sqrt{2/3}V_{\text{rat}} = 2694$ V, $I_B = \sqrt{2}I_{\text{rat}} = 503.5$ A and $f_B = f_{\text{rat}} = 50$ Hz. We also normalize the time axis t , with one time unit corresponding to $1/(2\pi f_B)$ seconds.

A. Reference Frames

All variables $\xi_{abc} = [\xi_a \ \xi_b \ \xi_c]^T$ in the three-phase system (abc) can be transformed to $\xi_{dq} = [\xi_d \ \xi_q]^T$ in the orthogonal rotating dq reference frame through $\xi_{dq} = \mathbf{K}(\varphi) \xi_{abc}$ with

$$\mathbf{K}(\varphi) = \frac{2}{3} \begin{bmatrix} \cos(\varphi) & \cos(\varphi - \frac{2\pi}{3}) & \cos(\varphi + \frac{2\pi}{3}) \\ -\sin(\varphi) & -\sin(\varphi - \frac{2\pi}{3}) & -\sin(\varphi + \frac{2\pi}{3}) \end{bmatrix}.$$

In here, φ denotes the angle between the a -axis of the three-phase system and the d -axis of the reference frame, which is aligned with the rotor flux vector. The reference frame rotates with the angular speed $\omega_{\text{fr}} = \omega_r = d\varphi/dt$, where ω_r is the electrical angular speed of the rotor.

The stationary $\alpha\beta$ reference frame is obtained by setting φ and ω_{fr} to zero. The d - and q -axes are then referred to as α - and β -axes, respectively, and we will write $\xi_{\alpha\beta} = \mathbf{K}(0)\xi_{abc}$.

B. Modeling

Consider the stator and rotor flux linkage vectors $\psi_{s,dq}$ and $\psi_{r,dq}$ in the rotating reference frame. Using these vectors as the state variables and treating the electrical angular speed of the rotor ω_r as a parameter, the continuous-time state-space model of the induction machine

$$\frac{d\psi_{s,dq}}{dt} = -R_s \frac{X_r}{D} \psi_{s,dq} - \omega_{\text{fr}} \mathbf{Q} \psi_{s,dq} + R_s \frac{X_m}{D} \psi_{r,dq} + \mathbf{v}_{s,dq} \quad (1a)$$

$$\frac{d\psi_{r,dq}}{dt} = R_r \frac{X_m}{D} \psi_{s,dq} - R_r \frac{X_s}{D} \psi_{r,dq} - (\omega_{\text{fr}} - \omega_r) \mathbf{Q} \psi_{r,dq} \quad (1b)$$

Voltage	3300 V	Stator resistance	$R_s = 0.0108$ pu
Current	356 A	Rotor resistance	$R_r = 0.0091$ pu
Real power	1.587 MW	Stator leak. react.	$X_{l_s} = 0.1493$ pu
Apparent power	2.035 MVA	Rotor leak. react.	$X_{l_r} = 0.1104$ pu
Stator frequency	50 Hz	Main reactance	$X_m = 2.349$ pu
Rotational speed	596 rpm	Total leak. react.	$X_\sigma = 0.2548$ pu
		dc-link voltage	$V_{\text{dc}} = 1.930$ pu
		dc-link capacitance	$X_c = 11.769$ pu

TABLE I: Rated values (left) and per unit parameters (right) of the drive system

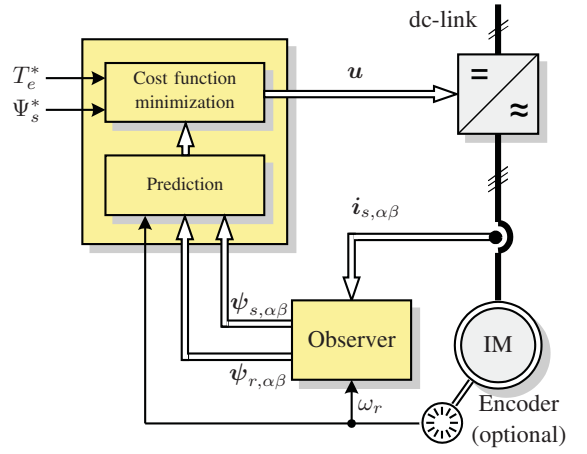


Fig. 2: Block diagram of the predictive torque and flux controller

can be obtained with the rotation matrix $\mathbf{Q} = \begin{bmatrix} 0 & -1 \\ 1 & 0 \end{bmatrix}$. The model parameters are the stator (rotor) resistance R_s (R_r), the stator (rotor) leakage reactance X_{l_s} (X_{l_r}) and the main reactance X_m . Furthermore, we define $X_s = X_{l_s} + X_m$, $X_r = X_{l_r} + X_m$ and $D = X_s X_r - X_m^2$. Note that all rotor quantities are referred to the stator circuit.

The stator voltage is given by

$$\mathbf{v}_{s,dq} = \frac{1}{2} V_{\text{dc}} \mathbf{K}(\varphi) \mathbf{u}, \quad (2)$$

where V_{dc} denotes the total dc-link voltage and $\mathbf{u} = [u_a \ u_b \ u_c]^T$ is the three-phase switch position. The switch positions in the three phase legs are u_a, u_b, u_c , which are restricted to the set $\{-1, 0, 1\}$ for a three-level converter.

The electromagnetic torque is given by

$$T_e = \frac{1}{\text{pf}} \frac{X_m}{D} \psi_{r,dq} \times \psi_{s,dq} = \frac{1}{\text{pf}} \frac{X_m}{D} (\psi_{rd} \psi_{sq} - \psi_{rq} \psi_{sd}), \quad (3)$$

where the operator \times refers to the cross product. The power factor is given by $\text{pf} = P_{\text{rat}}/S_{\text{rat}}$, with P_{rat} and S_{rat} referring to the rated real and apparent power, respectively. Note that the per unit system is based on the apparent power, whereas the real power relates to the electromagnetic torque. The inverse of the power factor in (3) ensures that $T_e = 1$ pu corresponds to rated torque.

The magnitude of the stator flux vector is defined as

$$\Psi_s = \|\psi_{s,\alpha\beta}\|_2 = \|\psi_{s,dq}\|_2 = \sqrt{\psi_{sd}^2 + \psi_{sq}^2}. \quad (4)$$

III. PREDICTIVE TORQUE AND FLUX CONTROL

The block diagram of the predictive torque and flux controller is shown in Fig. 2. The torque reference T_e^* is usually adjusted by an outer speed control loop. The reference of the stator flux magnitude is typically set to $\Psi_s^* = 1$ pu.

The predictive torque and flux controller tracks the references of the electromagnetic torque T_e^* and stator flux magnitude Ψ_s^* by manipulating the three-phase switch position $\mathbf{u} \in \{-1, 0, 1\}^3$. At the same time, the switching frequency is minimized.

A. Controller Model

The controller model predicts the electromagnetic torque and the magnitude of the stator flux vector at the next discrete time step $k+1$ as a function of the to-be-determined switch position $\mathbf{u}(k)$ at the current time step k . Consider the machine model (1) in the stationary orthogonal $\alpha\beta$ reference frame and let T_s denote the sampling interval. Integrating (1) from $t = kT_s$ to $t = (k+1)T_s$ with the forward Euler method leads to the discrete-time representation

$$\boldsymbol{\psi}_{s,\alpha\beta}(k+1) = \mathbf{A}_1 \boldsymbol{\psi}_{s,\alpha\beta}(k) + \mathbf{B}_1 \boldsymbol{\psi}_{r,\alpha\beta}(k) + \mathbf{B}_2 \mathbf{u}(k) \quad (5a)$$

$$\boldsymbol{\psi}_{r,\alpha\beta}(k+1) = \mathbf{A}_2 \boldsymbol{\psi}_{r,\alpha\beta}(k) + \mathbf{B}_3 \boldsymbol{\psi}_{s,\alpha\beta}(k). \quad (5b)$$

The system and input matrices are defined as

$$\begin{aligned} \mathbf{A}_1 &= \mathbf{I}(1 - R_s \frac{X_r}{D} T_s), \quad \mathbf{A}_2 = \mathbf{I}(1 - R_r \frac{X_s}{D} T_s) + \omega_r \mathbf{Q} T_s, \\ \mathbf{B}_1 &= R_s \frac{X_m}{D} \mathbf{I} T_s, \quad \mathbf{B}_2 = \frac{V_{dc}}{2} \mathbf{K}(0) T_s, \quad \mathbf{B}_3 = R_r \frac{X_m}{D} \mathbf{I} T_s, \end{aligned}$$

where \mathbf{I} denotes the two-dimensional identity matrix.

B. Optimization Problem

Over a one-step horizon, we define the cost function $J_1 = J_T + J_\Psi + J_{uT}$ with the terms

$$J_T = \lambda_T (T_e^*(k+1) - T_e(k+1))^2, \quad (6a)$$

$$J_\Psi = (1 - \lambda_T) (\Psi_s^*(k+1) - \Psi_s(k+1))^2, \quad (6b)$$

$$J_{uT} = \lambda_{uT} \|\Delta \mathbf{u}(k)\|_1. \quad (6c)$$

The first term penalizes the predicted deviation of the electromagnetic torque from its reference at time step $k+1$. Accordingly, the second term penalizes the predicted deviation of the stator flux magnitude from its reference. Both terms are penalized quadratically. The third term penalizes the switching effort at time step k , using the non-negative scalar weight λ_{uT} and the change in the switch position $\Delta \mathbf{u}(k) = \mathbf{u}(k) - \mathbf{u}(k-1)$.

The weight λ_T is introduced to discount the torque ripple and to prioritize the flux magnitude ripple, without changing the cost ratio between these two terms and the switching effort. To ensure that J_1 is non-negative, the weight λ_T is bounded between zero and one.

The optimization problem of the predictive torque and flux controller with reference tracking and a prediction horizon of one step can now be stated as

$$\mathbf{u}_{\text{opt}}(k) = \arg \underset{\mathbf{u}(k)}{\text{minimize}} J_T + J_\Psi + J_{uT} \quad (7a)$$

$$\text{subject to (5)} \quad (7b)$$

$$T_e(k+1) = \frac{1}{\text{pf}} \frac{X_m}{D} \boldsymbol{\psi}_{r,\alpha\beta}(k+1) \times \boldsymbol{\psi}_{s,\alpha\beta}(k+1) \quad (7c)$$

$$\Psi_s(k+1) = \|\boldsymbol{\psi}_{s,\alpha\beta}(k+1)\|_2 \quad (7d)$$

$$\mathbf{u}(k) \in \{-1, 0, 1\}^3, \quad \|\Delta \mathbf{u}(k)\|_\infty \leq 1. \quad (7e)$$

Note that $\|\Delta \mathbf{u}\|_\infty$ denotes the infinity-norm of the vector $\Delta \mathbf{u}$, which is defined as the component of $\Delta \mathbf{u}$ with the largest absolute value, i.e. $\|\Delta \mathbf{u}\|_\infty = \max(|\Delta u_a|, |\Delta u_b|, |\Delta u_c|)$.

One of the advantages of this control problem formulation is that the torque and flux references are constant during steady-state operation. Hence we may assume that $T_e^*(k+1) = T_e^*(k)$ and $\Psi_s^*(k+1) = \Psi_s^*(k)$.

C. Control Algorithm

The optimization problem (7) is typically solved by enumerating all switch positions and computing the cost for each one of them. The switch position at time step k with the minimum cost, $\mathbf{u}_{\text{opt}}(k)$, is by definition the optimal one, see for example [1] and [21].

Note that the rotor flux vector at time step $k+1$, $\boldsymbol{\psi}_{r,\alpha\beta}(k+1)$, needs to be computed only once using the state-update equation (5b). This is due to our choice of a one-step prediction horizon and the forward Euler discretization method, which neglects the coupling between the two flux vectors within the sampling interval.

D. Analysis

To improve the readability, we drop in this section the time dependence of the variables. To analyse the torque and flux controller, it is convenient to adopt the dq reference frame rotating in synchronism with the rotor flux.

By aligning the rotor flux vector with the d -axis, the torque expression (3) simplifies to

$$T_e = \frac{1}{\text{pf}} \frac{X_m}{D} \psi_{rd} \psi_{sq}. \quad (8)$$

With this, and recalling (4), the tracking error terms of the cost function can be expressed in terms of the d - and q -components of the stator flux vector. We rewrite (6a) and (6b) as

$$J_T = \lambda_T \left(\frac{1}{\text{pf}} \frac{X_m}{D} \psi_{rd} \right)^2 (\psi_{sq}^* - \psi_{sq})^2 \quad \text{and} \quad (9a)$$

$$J_\Psi = (1 - \lambda_T) (\|\boldsymbol{\psi}_{s,dq}^*\|_2 - \|\boldsymbol{\psi}_{s,dq}\|_2)^2. \quad (9b)$$

The reference of the stator flux vector is obtained from (8) and (4) as

$$\psi_{sq}^* = \text{pf} \frac{D}{X_m} \frac{T_e^*}{\psi_{rd}} \quad (10a)$$

$$\psi_{sd}^* = \sqrt{(\Psi_s^*)^2 - (\psi_{sq}^*)^2}. \quad (10b)$$

To visualize the two cost function terms in (9), consider the MV induction machine operating at nominal speed and rated torque. A geometrical representation of the torque error term J_T is provided in Fig. 3(a). The rotor flux vector is aligned with the d -axis. The reference of the stator flux vector corresponds to nominal torque and a fully magnetized machine. The contour lines of the torque error term J_T with the weight $\lambda_T = 0.052$ are shown as solid lines for the contour values 0.01, 0.02, ..., 0.08. The dash-dotted line refers to $J_T = 0$. Owing to (8), the contour lines are straight lines that are parallel to the rotor flux vector.

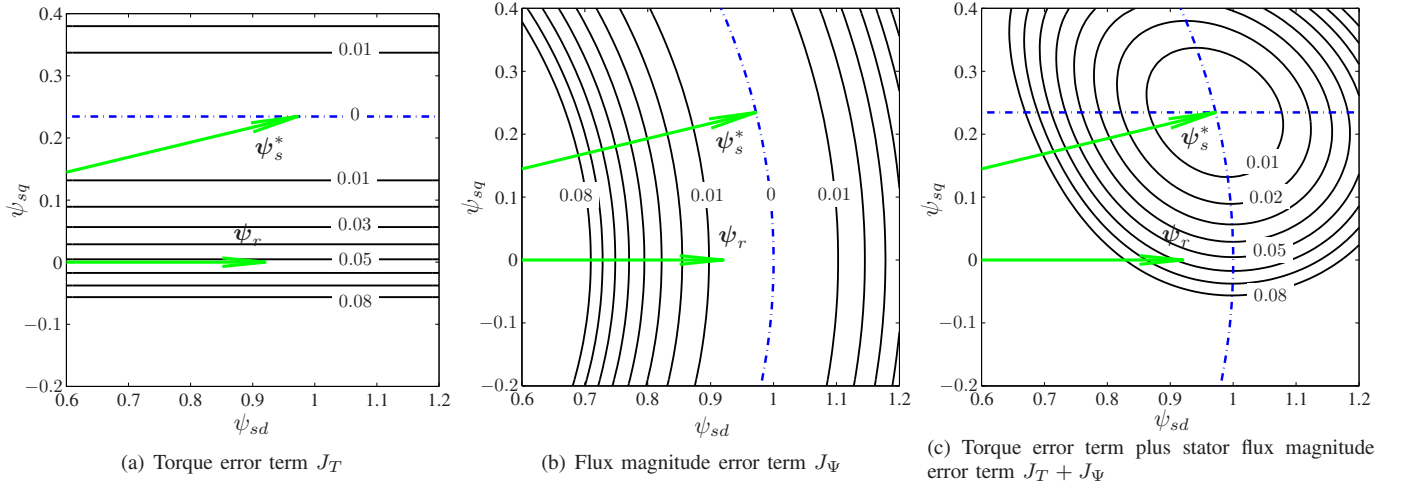


Fig. 3: Contour maps of the cost function terms of the predictive torque and flux controller in a plane spanned by the d - and q -components of the stator flux vector. The reference stator and rotor flux vectors are shown as arrows

Accordingly, the cost function term J_Ψ of the stator flux magnitude error is illustrated in Fig. 3(b). The contour lines of J_Ψ are depicted again for the values 0.01, 0.02, ..., 0.08. These contour lines form concentric circles that are centered on the origin of the dq reference frame. The dash-dotted line refers to $J_\Psi = 0$. Adding the two cost functions terms to $J_T + J_\Psi$ leads to the contour map shown in Fig. 3(c).

IV. PREDICTIVE CURRENT CONTROL

The current control problem is typically formulated in the stationary and orthogonal $\alpha\beta$ reference frame. The objective of the current controller is to manipulate the three-phase switch position \mathbf{u} such that the stator current $\mathbf{i}_{s,\alpha\beta}$ closely tracks its reference $\mathbf{i}_{s,\alpha\beta}^*$, while minimizing the switching frequency.

A. Controller Model

To predict future stator currents as a function of the three-phase switch position \mathbf{u} , we need to reformulate the state-space model (1). By adopting the stationary reference frame and inserting the expression $\psi_{s,\alpha\beta} = \frac{D}{X_r} \mathbf{i}_{s,\alpha\beta} + \frac{X_m}{X_r} \psi_{r,\alpha\beta}$ into (1a), we obtain after some lengthy algebraic manipulations the continuous-time state-space model of the stator currents

$$\frac{d\mathbf{i}_{s,\alpha\beta}}{dt} = -\frac{1}{\tau_s} \mathbf{i}_{s,\alpha\beta} + \left(\frac{1}{\tau_r} \mathbf{I} - \omega_r \mathbf{Q} \right) \frac{X_m}{D} \psi_{r,\alpha\beta} + \frac{X_r}{D} \mathbf{v}_{s,\alpha\beta}. \quad (11)$$

The transient stator and rotor time constants are defined as

$$\tau_s = \frac{X_r D}{R_s X_r^2 + R_r X_m^2} \quad \text{and} \quad \tau_r = \frac{X_r}{R_r}, \quad (12)$$

respectively.

The forward Euler discretization method leads to the discrete-time representation

$$\mathbf{i}_{s,\alpha\beta}(k+1) = \mathbf{A}_3 \mathbf{i}_{s,\alpha\beta}(k) + \mathbf{B}_4 \psi_{r,\alpha\beta}(k) + \mathbf{B}_5 \mathbf{u}(k) \quad (13)$$

with the system and input matrices

$$\begin{aligned} \mathbf{A}_3 &= \mathbf{I} \left(1 - \frac{1}{\tau_s} T_s \right), \quad \mathbf{B}_4 = \left(\frac{1}{\tau_r} \mathbf{I} - \omega_r \mathbf{Q} \right) \frac{X_m}{D} T_s, \\ \mathbf{B}_5 &= \frac{X_r}{D} \frac{V_{dc}}{2} \mathbf{K}(0) T_s. \end{aligned}$$

Equation (13) allows one to predict the stator current at the next time step $k+1$. The rotor flux dynamic is not required, because we adopted a one-step prediction horizon and the forward Euler discretization method.

B. Optimization Problem

We define the cost function $J_2 = J_I + J_{uI}$ with the stator current term J_I and the penalty on switching J_{uI} :

$$J_I = \|\mathbf{i}_{s,\alpha\beta}^*(k+1) - \mathbf{i}_{s,\alpha\beta}(k+1)\|_2^2, \quad (14a)$$

$$J_{uI} = \lambda_{uI} \|\Delta \mathbf{u}(k)\|_1. \quad (14b)$$

Note that $\|\xi_{\alpha\beta}\|_2^2 = \xi_\alpha^2 + \xi_\beta^2$ and $\lambda_{uI} \geq 0$.

The optimization problem underlying one-step predictive current control with reference tracking follows as

$$\mathbf{u}_{\text{opt}}(k) = \arg \underset{\mathbf{u}(k)}{\text{minimize}} J_I + J_{uI} \quad (15a)$$

$$\text{subject to (13)} \quad (15b)$$

$$\mathbf{u}(k) \in \{-1, 0, 1\}^3, \quad \|\Delta \mathbf{u}(k)\|_\infty \leq 1. \quad (15c)$$

C. Analysis

We compare the contour plots of the predictive torque and flux controller with those of the predictive current controller. As previously, we drop the time dependence of the variables and perform the analysis in the rotating dq reference frame. As the transformation from the stationary to the rotating reference frame is amplitude-invariant, we can rewrite (14a) as

$$J_I = \|\mathbf{i}_{s,dq}^* - \mathbf{i}_{s,dq}\|_2^2. \quad (16)$$

We can express the stator current as a linear combination of the stator and rotor flux vectors using $\mathbf{i}_{s,dq} = \frac{1}{D} (X_r \psi_{s,dq} -$

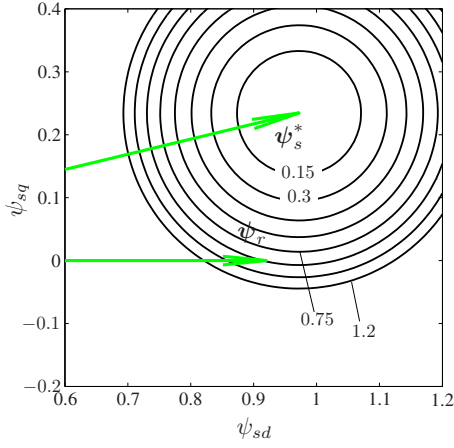


Fig. 4: Contour map of the current error term J_I of the predictive current controller

$X_m \psi_{r,dq}$). This allows us to rewrite the current error term (16) in terms of the stator flux:

$$J_I = \left(\frac{X_r}{D}\right)^2 \|\psi_{s,dq}^* - \psi_{s,dq}\|_2^2. \quad (17)$$

The contour lines of the current error term are shown in Fig. 4 as concentric circles around the stator flux reference. The contour lines are plotted for the values 0.15, 0.3, \dots , 1.2. Compared to the contour values used for the torque controller, these values are multiplied by a factor of 15.

V. WEIGHTING FACTOR SELECTION

When comparing the tracking error terms of the torque and flux controller (9) with that of the current controller (17), it is obvious that the cost functions of the two controllers are not equivalent. This observation is illustrated in Figs. 3(c) and 4 by the different shapes of the contour lines. Nevertheless, by appropriately tuning the weighting factors in the cost functions, a large degree of similarity between the two controllers can be achieved. Specifically, as shown in the following, λ_T can be chosen such that the contour lines of the torque controller approximate circles, particularly when the torque is close to zero.

To simplify the exposition in the following derivation, we set the torque reference to zero. Consider the stator flux vector

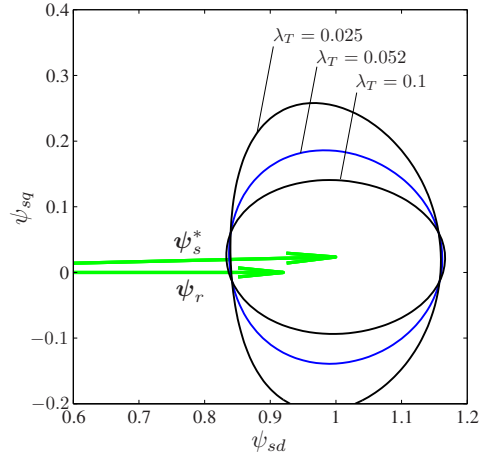
$$\psi_{s,dq} = \psi_{s,dq}^* + \begin{bmatrix} \psi_{\text{err}} \\ 0 \end{bmatrix} \quad (18)$$

with the flux error ψ_{err} in the d -axis. Note that $\psi_{sq}^* = 0$ because of our assumption that the torque reference is zero. According to (9), the cost is

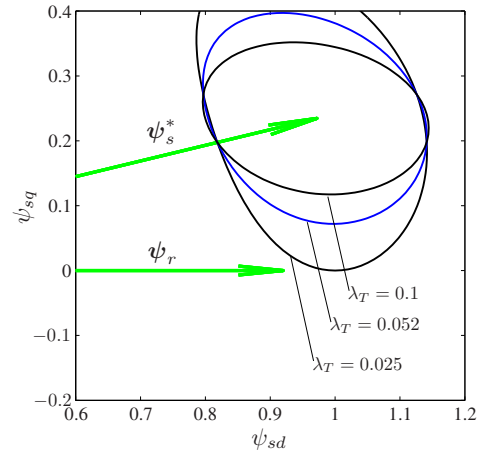
$$J_T + J_\Psi = (1 - \lambda_T) \psi_{\text{err}}^2. \quad (19)$$

Similarly, for a stator flux vector with the flux error ψ_{err} in the q -axis, the cost is

$$J_T + J_\Psi = \lambda_T \left(\frac{1}{\text{pf}} \frac{X_m}{D} \psi_{rd}\right)^2 \psi_{\text{err}}^2, \quad (20)$$



(a) Torque reference $T_e^* = 0.1$ pu



(b) Torque reference $T_e^* = 1$ pu

Fig. 5: Contour lines for the tracking error term $J_T + J_\Psi = 0.025$ of the predictive torque and flux controller for three different weighting factors λ_T

where we have neglected the minor contribution of J_Ψ . To achieve circular contour lines, both costs are required to be equal, which leads to

$$\lambda_T = \frac{(\text{pf}D)^2}{(\text{pf}D)^2 + (X_m \psi_{rd})^2}. \quad (21)$$

For the parameters of the considered drive system case study, we obtain $\lambda_T = 0.052$.

The validity of this choice is confirmed by Fig. 5(a), which depicts for three different λ_T the contour lines with the same cost $J_T + J_\Psi = 0.025$. When the torque reference is close to zero, $\lambda_T = 0.052$ leads to an effectively circular contour line. Variations in λ_T mostly affect the shape of the contour lines in the q -axis, which relates to the torque. Reducing λ_T , and hence the penalty on the torque error, widens the contour lines along the torque axis and increases the torque ripple. Conversely, when increasing λ_T and prioritizing the torque error, the torque ripple is reduced. In both cases, contour lines of elliptical shapes result. Note that variations of λ_T around 0.052 have only a minor effect on the contour lines along the d -

TABLE II: Comparison of the predictive torque and flux controller with the predictive current controller in terms of the current TDD I_{TDD} and torque TDD T_{TDD} . The switching penalties are chosen such that a switching frequency of approximately $f_{\text{sw}} = 220$ Hz results

Torque reference	Control scheme	Controller settings	I_{TDD} (%)	T_{TDD} (%)	f_{sw} (Hz)
$T_e^* = 0$	Torque and flux	$\lambda_T = 0.052, \lambda_{uT} = 0.198 \cdot 10^{-3}$	6.45	5.76	219
$T_e^* = 0$	Current	$\lambda_{uI} = 3 \cdot 10^{-3}$	6.38	5.57	220
$T_e^* = 1$	Torque and flux	$\lambda_T = 0.052, \lambda_{uT} = 0.198 \cdot 10^{-3}$	7.74	5.84	221
$T_e^* = 1$	Current	$\lambda_{uI} = 3 \cdot 10^{-3}$	6.69	5.51	222

axis, which relates to the stator flux magnitude and determines its ripple.

Increasing the torque reference from zero to one distorts the contour lines along the circular reference of the stator flux magnitude, as can be seen in Fig. 5(b). In particular, the circular shape of the contour line for $\lambda_T = 0.052$ becomes somewhat compromised. Nevertheless, as will be shown in the next section, the two predictive control schemes provide similar performance results at all torque setpoints, provided that λ_T and the penalties on switching are appropriately chosen.

Tuning of the latter is required, because the diameters of the (almost circular) reference tracking contour lines of the two control schemes differ; this can be seen when comparing Fig. 3(c) with Fig. 4. More specifically, errors in the stator flux vector are penalized more heavily for the current controller than for the torque controller. This implies that the switching penalty needs to be increased accordingly for the current controller to achieve the same switching frequency as the torque controller.

In the end, the *ratio* between the cost values of the tracking error and the switching penalty terms determines the controller response. To achieve a similar closed-loop behavior for the two predictive controllers, these ratios should be the same. We thus set

$$\frac{J_T + J_\Psi}{\lambda_{uT} \|\Delta \mathbf{u}(k)\|_1} = \frac{J_I}{\lambda_{uI} \|\Delta \mathbf{u}(k)\|_1}. \quad (22)$$

Consider again a zero torque reference, a stator flux error ψ_{err} in the d -axis and zero flux error in the q -axis as in (18). With (19) and (17), the expression (22) can be simplified to

$$\frac{(1 - \lambda_T) \psi_{\text{err}}^2}{\lambda_{uT}} = \left(\frac{X_r}{D}\right)^2 \frac{\psi_{\text{err}}^2}{\lambda_{uI}}. \quad (23)$$

This leads to

$$\lambda_{uI} = \left(\frac{X_r}{D}\right)^2 \frac{\lambda_{uT}}{1 - \lambda_T}. \quad (24)$$

We conclude that both control schemes issue very similar switching commands when their penalties are selected according to the following rules:

- For the torque controller, set λ_T according to (21). The second degree of freedom, the penalty on switching λ_{uT} , is selected such that the desired switching frequency is achieved.
- For the current controller, set its penalty on switching λ_{uI} according to (24).

As a result, the two predictive control schemes are expected to yield similar current and torque distortions for a given switching frequency. This hypothesis will be substantiated in the next section through closed-loop simulations.

VI. PERFORMANCE EVALUATION

For the performance evaluation of the predictive controllers, consider again the MV drive system case study of Sect. II. The operating point is at nominal speed, and the sampling interval is set to $T_s = 25 \mu\text{s}$. For the predictive torque and flux controller, we chose the penalty $\lambda_T = 0.052$. This choice ensures almost circular contour lines for the torque and flux error term and makes the reference tracking error term in the cost function of the torque and flux controller as similar as possible to that of the current controller. At rated torque, with the switching penalty $\lambda_{uT} = 0.198 \cdot 10^{-3}$, the predictive torque and flux controller yields a current total demand distortion (TDD) of 7.74%, a torque TDD of 5.84% and a device switching frequency of 221 Hz. The corresponding stator currents, torque and switch positions are shown in Fig. 6 over one fundamental period.

As shown in Table II, the TDDs and switching frequencies are similar to those obtained by the predictive current controller with the switching penalty $\lambda_{uI} = 3 \cdot 10^{-3}$. The latter closely matches the design guideline (24), i.e. $\lambda_{uI} = 16.25 \lambda_{uT}$. In particular, the current controller achieves the same switching frequency as the torque and flux controller (with $\lambda_{uT} = 0.198 \cdot 10^{-3}$).

At zero torque, both controllers achieve effectively the same current and torque TDDs, while at rated torque the current TDD deteriorates by 16% when using the torque and flux instead of the current controller. This worsening is due to the slightly non-circular shape of the contour lines for the stator flux error, which results in non-circular contour lines for the stator current error. The latter defines the current ripple and the current TDD. Nevertheless, at rated torque, the stator current ripple, torque ripple and the switching pattern are similar to those of the current controller. This can be seen when comparing Figs. 6 and 7. The instantaneous values are, however, different at rated torque, owing to the slightly different cost functions. Note that at zero torque, also the instantaneous values are very similar.

The similarity between the two control schemes is further underlined by Fig. 8, which shows the current and torque TDDs versus the switching frequency. At nominal speed and rated torque, and for switching frequencies in excess of 250 Hz, both schemes yield very similar current and torque TDDs for a given switching frequency, with the current controller slightly outperforming the torque and flux controller. This small difference becomes more pronounced at low switching frequencies.

Fig. 9(a) shows the influence λ_T has on the current TDD. The value of $\lambda_T = 0.052$ clearly minimizes the current TDD,

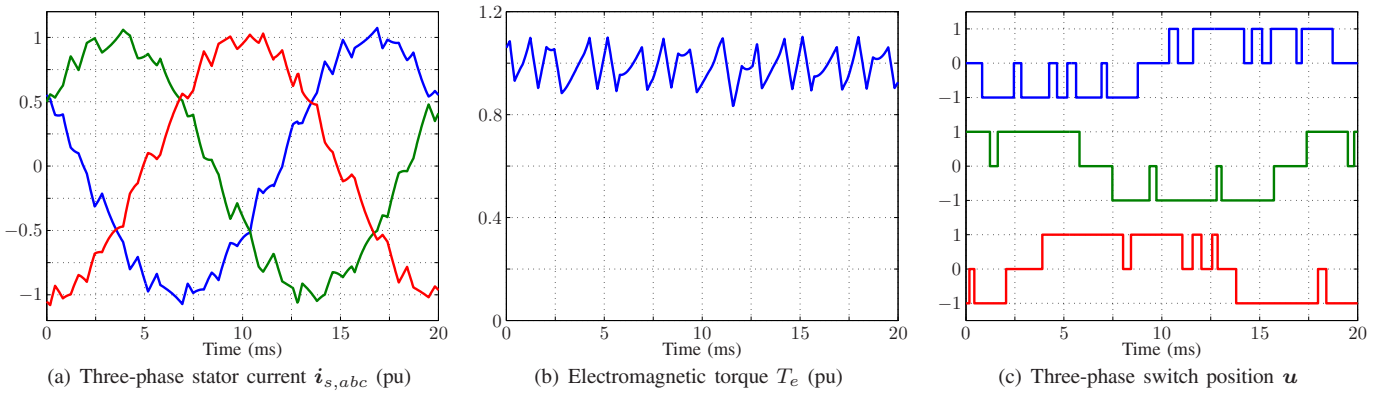


Fig. 6: Predictive torque and flux control during steady-state operation for $\lambda_T = 0.052$ and $\lambda_{uT} = 0.198 \cdot 10^{-3}$, with $I_{TDD} = 7.74\%$ and $f_{sw} = 221$ Hz

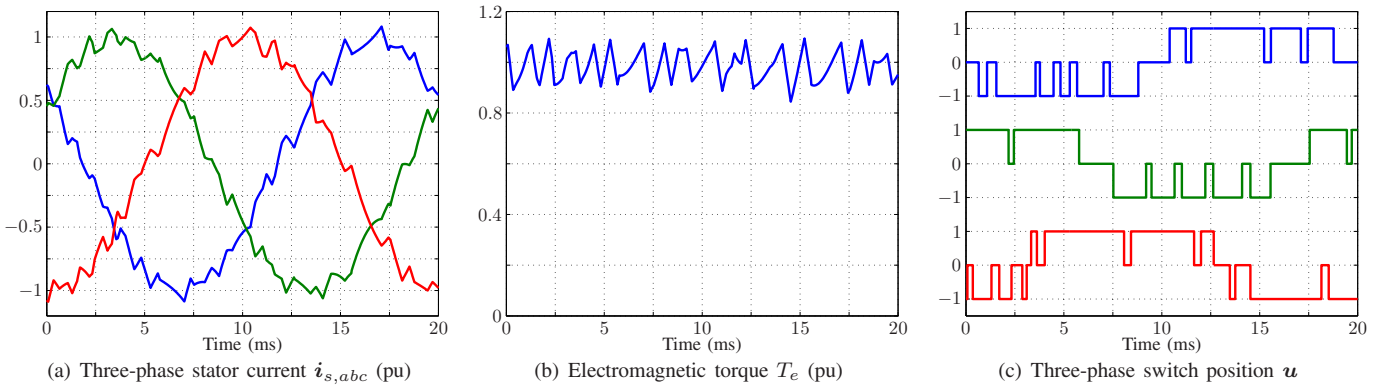


Fig. 7: Predictive current control during steady-state operation for $\lambda_{uI} = 3 \cdot 10^{-3}$, with $I_{TDD} = 6.69\%$ and $f_{sw} = 222$ Hz

confirming the cost function analysis provided in Sect. V. For the torque TDD, however, the relatively small penalty of $\lambda_T = 0.052$ leads to relatively large torque distortions, as shown in Fig. 9(b). Increasing the penalty fivefold to 0.25, for example, halves the torque TDD throughout the considered switching frequency range from 50 Hz to 1.2 kHz. This reduction in the torque TDD, however, comes at the price of pronounced current distortions, see Fig. 9(a). Nevertheless, for some applications, very low torque TDDs might be beneficial. The parameter λ_T endows the torque controller with a degree of freedom to facilitate this.

When the two predictive controllers operate at low switching frequencies, the switching frequency tends to lock into integer multiples of the fundamental frequency, such as 50, 100, \dots , 250 Hz, despite significant variations in the switching penalty. This phenomenon can be seen in Figs. 8 and 9. It implies a certain degree of periodicity in the switching actions and a somewhat discrete current spectrum. This feature is more pronounced in the case of long prediction horizons, as discussed and analyzed in [22].

VII. CONCLUSIONS

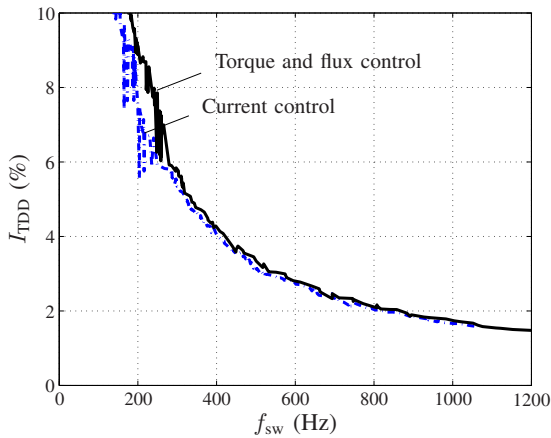
We conclude that, in general, the predictive torque and flux controller and the current controller yield similar performance metrics at steady-state operation, provided that the weighting factors are chosen in accordance with the two algebraic design

guidelines stated in this paper. The first guideline (21) ensures that the torque and flux controller achieves minimum current distortions per switching frequency. The second guideline (24) ensures a strong performance similarity between the two control schemes.

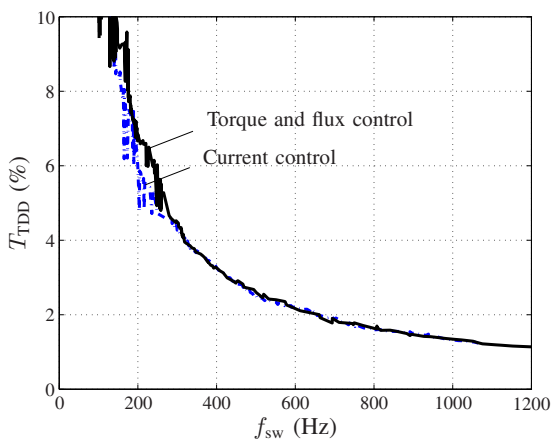
In light of this strong similarity, additional criteria could be considered when deciding between the predictive current controller and the predictive torque and flux controller. Besides the harmonic performance, relevant criteria include the robustness to parameter variations, the simplicity of the outer control loops and the ease with which current constraints could be added.

REFERENCES

- [1] P. Cortés, M. P. Kazmierkowski, R. M. Kennel, D. E. Quevedo, and J. Rodríguez, "Predictive control in power electronics and drives," *IEEE Trans. Ind. Electron.*, vol. 55, pp. 4312–4324, Dec. 2008.
- [2] S. Kouro, P. Cortés, R. Vargas, U. Ammann, and J. Rodríguez, "Model predictive control—A simple and powerful method to control power converters," *IEEE Trans. Ind. Electron.*, vol. 56, pp. 1826–1838, Jun. 2009.
- [3] J. Rodríguez, M. P. Kazmierkowski, J. R. Espinoza, P. Zanchetta, H. Abu-Rub, H. A. Young, and C. A. Rojas, "State of the art of finite control set model predictive control in power electronics," *IEEE Trans. Ind. Informatics*, vol. 9, pp. 1003–1016, May 2013.
- [4] J. Rodríguez, J. Pontt, C. Silva, P. Cortés, U. Ammann, and S. Rees, "Predictive direct torque control of an induction machine," in *Proc. IEEE Power Electron. and Motion Control Conf.*, (Riga, Latvia), 2004.

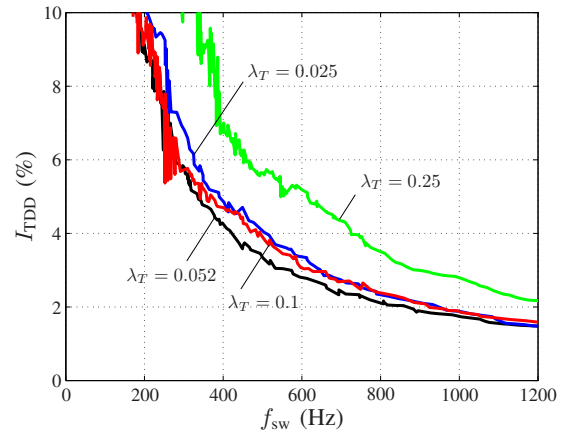


(a) Current TDD versus switching frequency

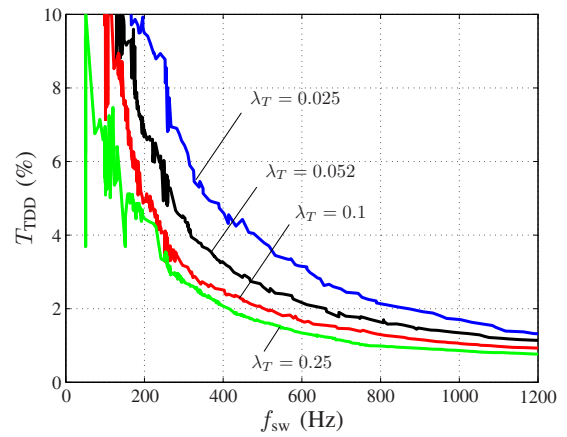


(b) Torque TDD versus switching frequency

Fig. 8: Predictive torque and flux control with $\lambda_T = 0.052$ is compared with predictive current control when operating at nominal speed and rated torque



(a) Current TDD versus switching frequency



(b) Torque TDD versus switching frequency

Fig. 9: Predictive torque and flux control is considered with different torque penalties λ_T when operating at nominal speed and rated torque

[5] H. Miranda, P. Cortés, J. I. Yuz, and J. Rodríguez, "Predictive torque control of induction machines based on state-space models," *IEEE Trans. Ind. Electron.*, vol. 56, pp. 1916–1924, Jun. 2009.

[6] P. Cortés, S. Kouro, B. L. Rocca, R. Vargas, J. Rodríguez, J. I. León, S. Vazquez, and L. G. Franquelo, "Guidelines for weighting factors design in model predictive control of power converters and drives," in *Proc. IEEE Int. Conf. Ind. Technol.*, 2009.

[7] S. Thielemans, T. Vyncke, and J. Melkebeek, "Weight factor selection for model-based predictive control of a four-level flying-capacitor inverter," *IET Power Electron.*, vol. 5, pp. 323–333, Mar. 2011.

[8] R. Vargas, U. Ammann, B. Hudoffsky, J. Rodríguez, and P. Wheeler, "Predictive torque control of an induction machine fed by a matrix converter with reactive input power control," *IEEE Trans. Power Electron.*, vol. 25, pp. 1426–1438, Jun. 2010.

[9] J. Rodríguez, R. M. Kennel, J. R. Espinoza, M. Trincado, C. A. Silva, and C. A. Rojas, "High-performance control strategies for electrical drives: An experimental assessment," *IEEE Trans. Ind. Electron.*, vol. 49, pp. 812–820, Feb. 2012.

[10] P. Zanchetta, "Heuristic multi-objective optimization for cost function weights selection in finite states model predictive control," in *Workshop on Pred. Control of Electr. Drives and Power Electron.*, (Munich, Germany), Oct. 2011.

[11] S. A. Davari, D. A. Khaburi, and R. Kennel, "An improved FCS-MPC algorithm for an induction motor with an imposed optimized weighting factor," *IEEE Trans. Power Electron.*, vol. 27, pp. 1540–1551, Mar. 2012.

[12] C. Rojas, J. Rodríguez, F. Villarroel, J. Espinoza, C. Silva, and M. Trincado, "Predictive torque and flux control without weighting factors," *IEEE Trans. Ind. Electron.*, vol. 60, pp. 681–690, Feb. 2013.

[13] K. Hasse, "Zum dynamischen Verhalten der Asynchronmaschine bei

Betrieb mit variabler Ständerfrequenz und Ständerspannung," *ETZ-A*, vol. 89, pp. 387–391, 1968.

[14] S. Müller, U. Ammann, and S. Rees, "New modulation strategy for a matrix converter with a very small mains filter," in *Proc. IEEE Power Electron. Spec. Conf.*, (Acapulco, Mexico), Jun. 2003.

[15] J. Rodríguez, J. Pontt, C. Silva, M. Salgado, S. Rees, U. Ammann, P. Lezana, R. Huerta, and P. Cortés, "Predictive control of three-phase inverter," *IET Electronics Letters*, vol. 40, pp. 561–563, Apr. 2004.

[16] J. Rodríguez, J. Pontt, C. A. Silva, P. Correa, P. Lezana, P. Cortés, and U. Ammann, "Predictive current control of a voltage source inverter," *IEEE Trans. Ind. Electron.*, vol. 54, pp. 495–503, Feb. 2007.

[17] R. Vargas, P. Cortés, U. Ammann, J. Rodríguez, and J. Pontt, "Predictive control of a three-phase neutral-point-clamped inverter," *IEEE Trans. Ind. Electron.*, vol. 54, pp. 2697–2705, Oct. 2007.

[18] J. Holtz, "Pulsewidth modulation—A survey," *IEEE Trans. Ind. Electron.*, vol. 32, pp. 410–420, Dec. 1992.

[19] T. Geyer, "Model predictive direct current control: Formulation of the stator current bounds and the concept of the switching horizon," *IEEE Ind. Appl. Mag.*, vol. 18, pp. 47–59, Mar./Apr. 2012.

[20] T. Geyer, "A comparison of control and modulation schemes for medium-voltage drives: Emerging predictive control concepts versus PWM-based schemes," *IEEE Trans. Ind. Appl.*, vol. 47, pp. 1380–1389, May/Jun. 2011.

[21] T. Geyer, *Model predictive control of high power converters and industrial drives*. London, UK: Wiley, Oct. 2016.

[22] T. Geyer and D. E. Quevedo, "Performance of multistep finite control set model predictive control for power performance," *IEEE Trans. Power Electron.*, vol. 30, pp. 1633–1644, Mar. 2015.